Light Yield Calibration in MicroBooNE

The MicroBooNE Collaboration

MICROBOONE-NOTE-1120-TECH,
Email: MICROBOONE_INFO@fnal.gov

Abstract

The MicroBooNE detector is a Liquid Argon Time Projection Chamber (LArTPC) located along the Booster Neutrino Beam (BNB) at Fermilab. Its primary physics goal is to contribute to addressing the elusive short-baseline MiniBooNE low energy excess. MicroBooNE records and utilises both the ionisation charge and scintillation light produced inside the TPC to select and reconstruct neutrino interactions. The scintillation light collected using a plane of PhotoMultiplier Tubes (PMTs) is also used for accurate event timing and cosmic muon rejection with the latter being an important background for detectors, such as MicroBooNE, located on the surface. A good understanding of light modeling and its related systematic uncertainties is crucial to evaluate their impact on physics analyses. The experience acquired from MicroBooNE regarding how the stability of the scintillation light behaves and evolves during the 5 years of the primary physics run will be discussed as well as the calibration method used. This experience will help with understanding the physics of scintillation light in LArTPCs for the future long-running Short-Baseline Neutrino (SBN) and Deep Underground Neutrino Experiment (DUNE) programs.

Contents

1 Introduction

Liquid Argon Time Projection Chambers (LArTPCs) are being used by multiple neutrino experiments due to their inherent active calorimetry capabilities and their excellent 3D tracking of charged particles within the active volume. Segmentation of the charge readout in the order of a few millimeters allows for precise energy reconstruction as well as enabling particle identification (PID).

Liquid argon is also a prolific scintillator. In the absence of electrical field, on average, 40,000 Vacuum Ultra-Violet (VUV) photons are emitted per MeV of energy loss [1]. Emitted photons from the de-excitation of the argon dimers can travel across the drift volume of LArTPCs much faster than the ionisation charge produced by charged particles inside the argon. The detection time of the photons can be used to identify the initial time, t_0, of the interaction of a neutrino candidate and help determine the absolute drift coordinate of non-beam related events inside the TPC. Because of the good timing resolution of the scintillation light response, neutrino interactions that produce a sufficient number of photons are used to trigger the readout of the detector. In MicroBooNE, events with $\sim$5 Photo-electrons (PEs) trigger the data acquisition system to save the event to tape. A second software trigger of $\sim$20 PE is also applied to remove events with low amounts of light as well as help to reject some of the cosmic ray background happening in beam-spills where there are no neutrino interactions.

To enable the flagship physics of MicroBooNE - the search for the low energy excess (LEE) (see [2]) - and MicroBooNE's broader neutrino and BSM physics capabilities, both the physics light model and the modeling of the light response of the detector must be well understood. As such, it is important to monitor the light yield over the course of the physics runs to allow

any changes in the response over time to be accounted for using data-driven corrections.

2 The MicroBooNE Detector

The MicroBooNE detector [3] is a rectangular LArTPC sitting at the surface along the Booster neutrino beam in the Fermi National Accelerator Laboratory (FNAL). MicroBooNE is 2.6 m wide along the drift direction, 2.3 m high, and 10.4 m long along the beam direction with the TPC consisting of an active mass of 85 tonnes. A series of 3 planes of sense-wires, placed in front of the light detection system, allow the TPC to measure the charge deposited inside the active volume by charged particles interacting with the argon.

2.1 Light Detection System

MicroBooNE uses an array of 32 8" diameter Hamamastu R912-02mod cryogenic photomultiplier tubes (PMTs) arranged in 5 rosettes as shown in Figure 1. Each of the 32 PMTs are placed behind a circular acrylic plate that is coated with a layer of tetraphenyl butadiene (TPB), a wavelength-shifter. The TPB layer can absorb the LAr VUV emitted light ($\sim$128 nm) and re-emit it in the visible range, peaking at about 430 nm, where the PMTs have a high quantum efficiency. Curves showing the absorption and re-emission of the light by the TPB layer are shown in Figure 2 for comparison.

Nominally, the PMTs are operated at a high voltage around 1,300 V resulting in an electronic gain of $\approx 10^7$. Each time the PMT system is turned off, the gains are re-calibrated by performing minor adjustments to the high voltage (see [4] for more information on the gain calibration of the MicroBooNE PMTs).

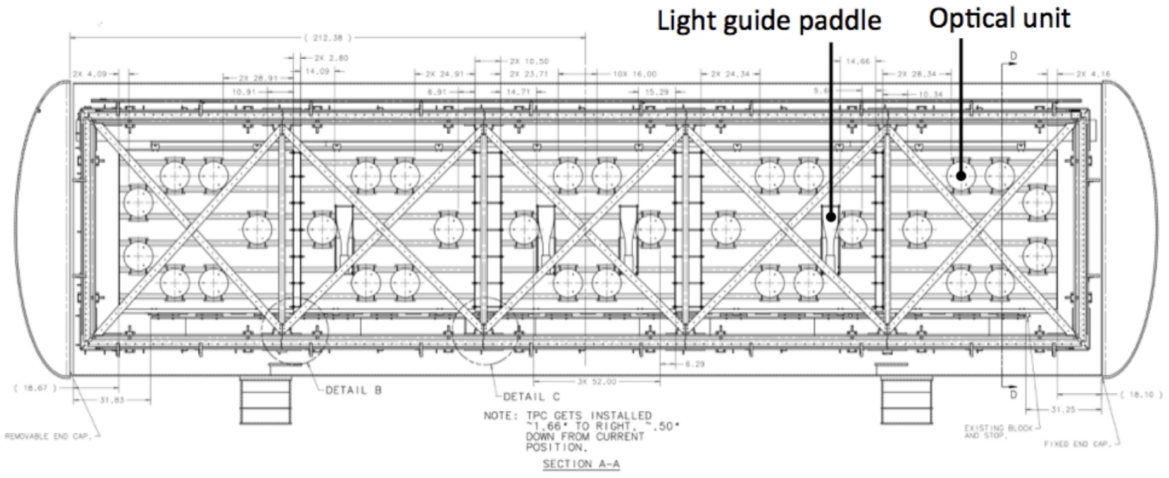

Figure 1: Schematic of a cut out the MicroBooNE TPC showing the placement of the light collection system. Figure taken from [3].

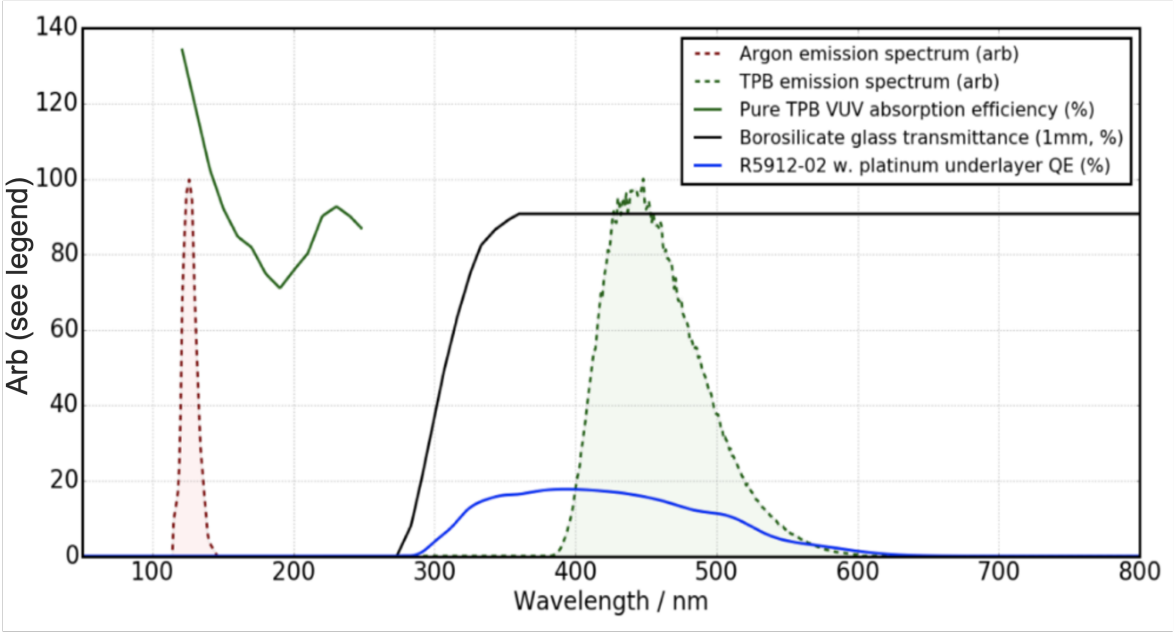

Figure 2: Spectrum of the LAr scintillation, TPB absorption and emission, and the PMT quantum efficiency in terms of the wavelengths. Figure taken from [3].

3 Time-Based Light Yield Stability Measurement

It is important to track the performance of the light detection system due to time-dependent effects such as changing amounts of impurities in the argon, ageing of the PMTs and/or degradation of the TPB. While it can be very difficult to disentangle these various effects, a targeted calibration campaign can reduce the impact of these factors on the analysis results. This can be done by looking at the light yield stability over time and using the comparative results as time-dependent corrections.

3.1 Data sample and selection

The measurement is performed using samples of through-going cosmic-ray-induced muon tracks that cross either the anode or the cathode of the detector, referred to as anode or cathode piercing tracks (ACPT). These samples are useful for the light calibration since they are minimally dependent on the light for reconstruction. Instead, tracks crossing the anode or the cathode of the detector can be identified through the charge information alone based on the expected position of the anode or cathode in the drift direction relative to the trigger time [5]. This helps to minimise any biases that could occur during reconstruction if the light response varies over time.

The ACPT samples are divided into two sets, each illustrated in Figure 3 (left), depending on whether they are anode-piercing (APT) or cathode-piecing (CPT). Tracks are selected that either enter the top of the detector and exit through the anode/cathode, or enter the anode/cathode and exit through the bottom of the detector. An example event display of a selected cathode-piercing track is shown in Figure 3 (right), where the position of the cathode

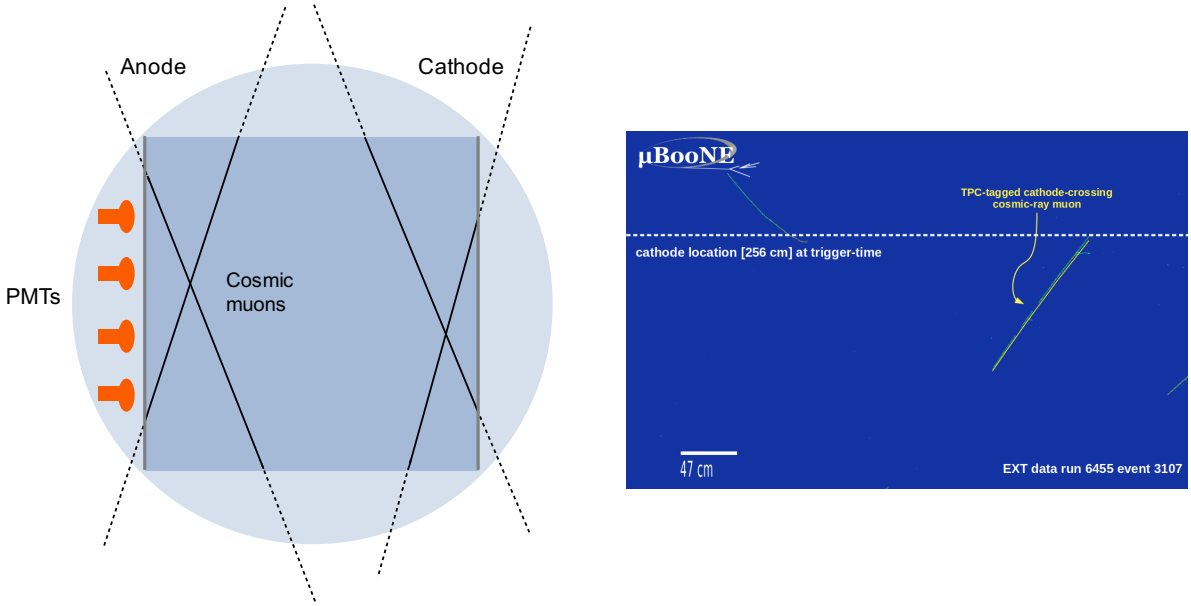

Figure 3: Left: illustration of the cosmic-ray-induced muon tracks selected in the anode piercing and cathode piercing samples. Right: example event display of a selected cathode piercing track. The white dashed line shows the position of the cathode.

is shown by the dashed white line. The resulting selected tracks are distributed throughout the entire length of the detector in the beam direction and have no threshold applied to the individual PMT readout. Once selected using the TPC, a simplified flash-matching is then performed to improve the purity of the sample. Compatibility between the reconstructed flash and track positions is required by imposing that the flash center and track center in the beam direction fall within 100 cm of each other. Several quality cuts are then applied in order to remove poorly reconstructed tracks and tracks that are outliers in length, amount of light or position. Tracks are removed that have: length $L < 40\,\text{cm}$ or $L > 400\,\text{cm}$; total number of photons $N_{PE} > 10000$ for APT or $N_{PE} > 1000$ for CPT; or that start or end within 50 cm of the cathode for APT or anode for CPT.

Since MicroBooNE is a surface detector it is exposed to a high flux of these cosmic-ray-induced muons, allowing a high statistics time-dependent measurement of the light response to be performed. The ACPT sample spans between March 2016 and March 2020, covering the physics run 1-5 periods along with the summer shutdowns between each run. The distribution of the data over time is shown in Figure 4. The run periods are as follows:

1. Run 1 $\Longrightarrow$ 2015-10 to 2016-07,
2. Run 2 $\Longrightarrow$ 2016-10 to 2017-07,
3. Run 3 $\Longrightarrow$ 2017-10 to 2018-07,
4. Run 4 $\Longrightarrow$ 2018-10 to 2019-07,
5. Run 5 $\Longrightarrow$ 2019-10 to 2020-03.

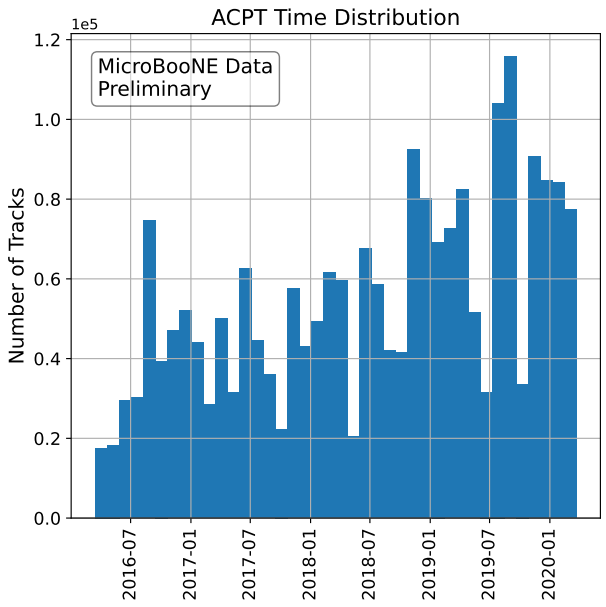

Figure 4: Distribution of ACPT data sample over time.

Once data quality cuts are applied, we select approximately 850,000 anode-piercing tracks and 575,000 cathode-piercing tracks.

Two periods of low argon purity are also removed from the samples. These span from September 22nd to October 6th 2018 and from February 20th - Mar 1st 2020. During these periods the electron lifetime was insufficient for the ionisation charge to drift from the cathode to the anode. This results in APT appearing shorter, since only the charge close to the anode is seen, resulting in them appearing to have a disproportionately large light yield in terms of PE/cm. In addition, during these periods no CPT are reconstructed.

3.2 Method and results

The selected through-going muon tracks are approximately minimally ionising for the entirety of their path in the detector. The light yield of each muon is therefore evaluated in terms of the total number of photons observed across all PMTs divided by the length of the muon track, in PE/cm. Since the PMTs are located only at the anode of the detector, the light yield is highly non-uniform in the drift direction. Therefore, the anode-piercing tracks result in significantly more light being observed than the cathode-piercing tracks. To allow comparison between the two sub-samples to be performed, the relative change in the light yield is assessed over time rather than the absolute yield.

The APT and CPT samples are divided into bins in time. To reliably assess the variation of the light yield over time, the bin width is allowed to vary to ensure the same number of tracks is present in each bin. It was found that 5000 tracks per bin provided sufficient statistics. The light yield in each bin, in PE/cm, was then quantified by evaluating the truncated median of the distribution within that bin. This allows the peak of the distribution to be

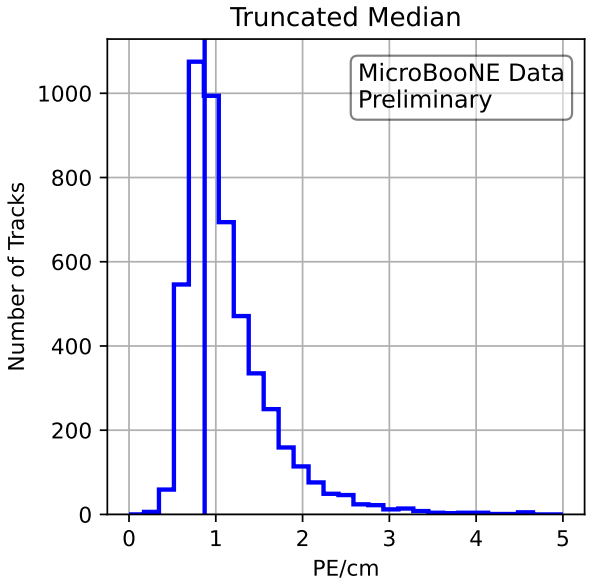

Figure 5: Example distribution in PE/cm for cathode-piercing tracks contained within a single time bin. The light yield is quantified using the truncated median of the distribution, shown by the vertical line.

identified without being skewed by outlier events. An example of the distribution within a single time bin and the truncated median algorithm being applied is shown in Figure 5.

The percentage change in the light response over time is shown in Figure 6 for the anode-piercing tracks (black) and cathode-piercing tracks (red). The light yield is observed to decline significantly in between September 2016 and January 2018 for both the anode-piercing and cathode-piercing tracks. It then remains approximately stable until the end of MicroBooNE's physics runs in March 2020. The amplitude of the decline is significantly different for the anode-piercing and cathode-piercing tracks: approximately 25% at the anode, and 45-50% at the cathode. The cause of the light response decline, and the difference in the size of the decline between the anode and cathode piercing tracks, is the subject of active investigation.

Similar studies leveraging other samples are currently ongoing [6]. These will help to provide further understanding of the light response stability.

3.3 Calibration

Since the light response varies substantially over time, a time-dependent calibration is necessary to model it. To develop the calibration the sample is re-binned to have constant bin width in time. Since the cause of the light response decline and the difference between the anode and the cathode are unknown, the calibration values are taken as the midpoint between the APT and CPT measurements with an uncertainty corresponding to half of the difference between them. This avoids the need to assume a particular model for the an-

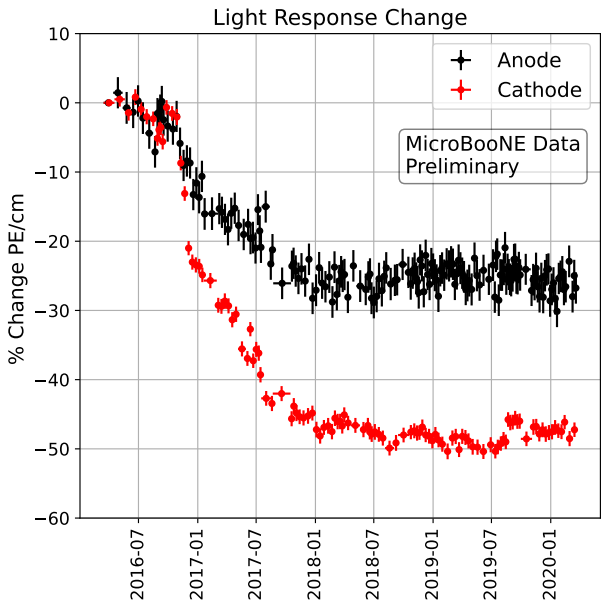

Figure 6: Percentage change in the light yield over time for the anode piercing tracks (black) and cathode piercing tracks (red).

ode/cathode difference, such as absorption, and instead allows the range of the decline to be evaluated as a systematic uncertainty in analyses. The resulting calibration values are shown in Figure 7.

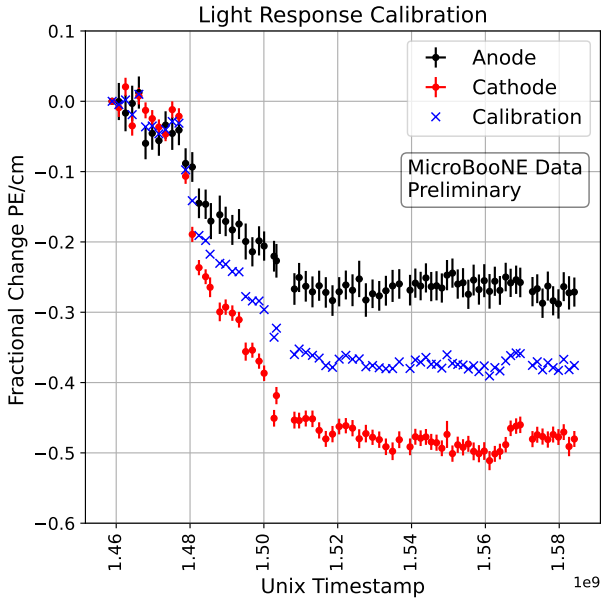

Figure 7: Light response decline calibration (blue) determined from the midpoint between the observed declines for anode piercing and cathode piercing tracks.

4 Discussion of the Light Yield Decline

As seen in Figure 6, after the first physics run the light yield declines significantly between approximately September 2016 and January 2018 for both tracks at the anode and the cathode. It then stabilises for the remaining physics runs until March 2020. It is important to understand and account for any effects that this may have on physics analyses.

4.1 Potential Sources of Light Decline

The cause of the light decline is currently the subject of active investigation. One possible cause could be the introduction of impurities into the argon in September 2016 that would then have stabilized over time. These impurities could both quench the slow component of the argon scintillation light, reducing the amount of light produced, and absorb the light during propagation to the PMTs, resulting in a position dependence in the observed light decline [7, 8, 9, 10, 11]. These impurities, however, must not affect the ionization charge since no decrease of the electron lifetime has been observed in the same time period.

A first study of the contaminants present in the MicroBooNE detector has been performed by taking a sample of the argon directly from the cryostat. This sample was then sent to CIEMAT in Spain to perform a measurement using an inductively coupled plasma mass spectrometer [12]. The MicroBooNE argon was compared with two standard high purity commercial argon samples (N50 and N60 from AirLiquide) as references. Preliminary results indicate that the MicroBooNE argon sample contains more nitrogen than the two references. They also show that there is a non-insignificant amount of xenon and krypton both at larger concentration than the reference argon. The exact concentrations of the three top contaminants are still unknown and are under further analysis. Studies on their effect on the light yield in MicroBooNE are also underway.

4.2 Light Yield Decline as a Systematic Uncertainty

To properly account for both light mis-modelling and the light decline, MicroBooNE generates three distinct light specific detector variation samples which generate three different light yield maps. They are as follows:

1. Overall 25% decrease,
2. Rayleigh scattering,
3. Attenuation (for Run 3 only).

Overall 25% Decrease

Light mis-modelling is generally not time-dependent but can still affect the overall light yield. As such, events producing light at the anode and at the cathode were compared both in data and simulation. Ratios (simulation/data) at different value of drift distance were calculated for the amount of photo-electrons measured per centimeter of track-length

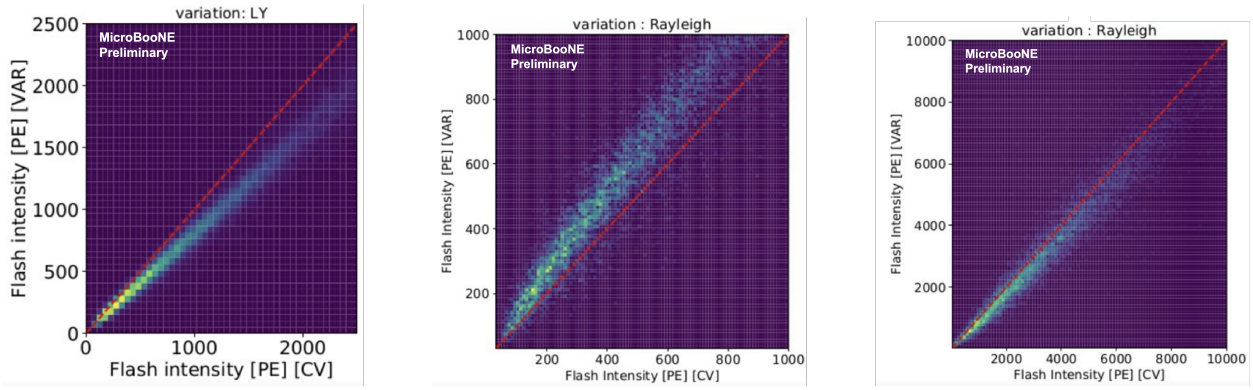

(a) 25% light yield down (b) Rayleigh at low X (c) Rayleigh at high X

Figure 8: Comparison between the amount of PE of the same events between the standard sample (CV) and two of the light yield variation samples

(PE/cm). These ratios showed an average 25% over-prediction in the simulation thus the necessity of producing a 25% down light yield map to account for the differences.

Rayleigh scattering

MicroBooNE's current simulation uses a Rayleigh scattering length of 60 cm. Recent measurements have shown that the scattering length might be closer to 100 cm [13]. As such, position-dependent light yield variations due to Rayleigh scattering were studied using a MicroBooNE-like geometry. The results of those studies were incorporated in the visibility map simulation to produce a map where each voxel's response is scaled by the ratio between the simulation of a 120 cm vs. a nominal 60 cm scattering length.

Attenuation

The most significant light yield decline occurs between run 1 and run 3 of MicroBooNE's physics runs. An attenuation variation light map was created to allow comparison between these two time periods. This light decline is seen to have a dependence on the position of the interaction in the drift direction which may correspond to attenuation caused by quenching combined with absorption. The variation map was created using a 20% quenching and 8 meters absorption length at the anode (lowest drift distance) and a 40% quenching and 13 meters absorption length at the cathode (highest drift distance) to evaluate a systematic uncertainty due to these effects. These values are conservative and approximate a simplified scenario.

Regardless of the true source of the light yield decline, MicroBooNE's detector systematic variations account for the differences observed over time with the light yield as well as the mis-modelling of the light properties. Figure 8 shows comparisons between the amount of light in the standard visibility maps and the 25% light yield down variation (left) and Rayleigh scattering variation (middle, right) samples. In the first case the amount of light is simply reduced while for the latter there are differences at low and high drift distances (X).

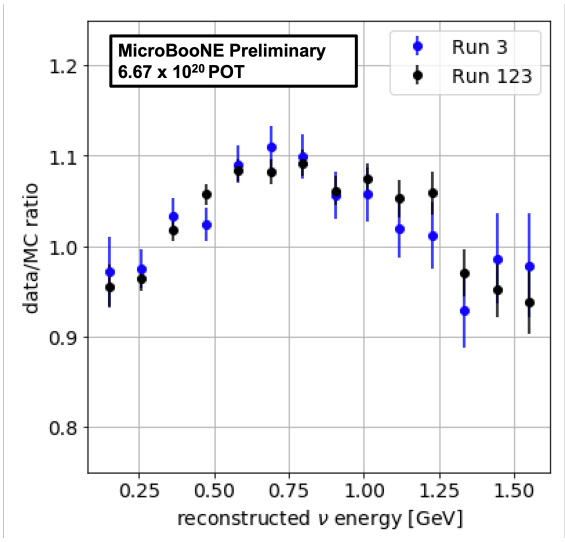

Figure 9: Statistical-only comparison of selected ν_μ events during runs 1, 2 and 3 compared to events selected during run 3 only.

4.3 Effects of the Light Yield Decline on Analyses

The primary use of scintillation light in MicroBooNE is to trigger on and identify neutrino interactions in the detector, rejecting cosmic-ray backgrounds out-of-time with respect to the beam. While selection cuts on event samples vary, most analyses use a ∼20 PE prompt / ∼50 PE total light threshold on events. It is thus important to study if the light yield decline has an impact on the number of neutrino candidates selected.

As a test case, the ratio between the number of events selected in data and simulation for the ν_μ selection in [14] can be studied. Looking at the selected ν_μ event candidates in runs 1, 2 and 3 vs. the ones in only run 3 in Figure 9 shows consistent results between the different data-sets obtained at different times. This indicates that the agreement between simulation and data for selected neutrino interactions is not significantly impacted by the light response decline between run 1 and run 3. Any potential impact on the number of neutrinos being selected is therefore modelled effectively by the time-dependent calibration shown in Figure 7.

Another crosscheck can be performed by looking at the reconstructed π^0 mass for the first three physics run separately. Figure 10 shows the π^0 mass peak remains unchanged across runs giving confidence in the stability of event reconstruction and selection over time. In addition, the number of selected BNB data events is approximately the same between the three runs once the differences in POT are accounted for. This indicates that the number of selected neutrinos is not significantly impacted by the light response decline between run 1 and run 3.

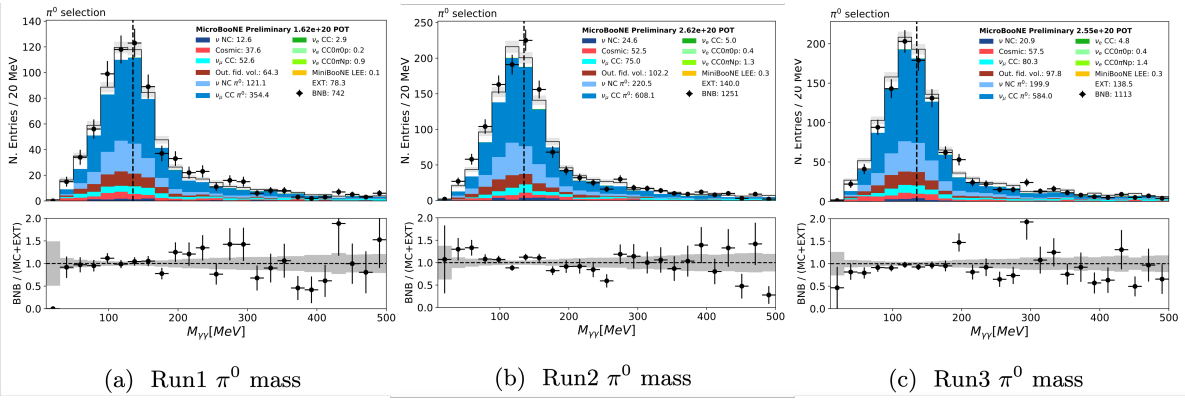

(a) Run1 π^0 mass (b) Run2 π^0 mass (c) Run3 π^0 mass

Figure 10: Comparison of the π^0 mass for runs 1, 2, and 3 in data and simulation. The mass peak remains stable across all three runs despite the light response decline.

5 Conclusion

MicroBooNE is the longest running neutrino LArTPC to date. To study the stability of the light response over time samples of anode-piercing and cathode-piercing muon tracks have been used. The light response was observed to decline significantly between September 2016 and January 2018: by approximately 25% at the anode and 45-50% at the cathode. A time dependent light response calibration has been developed using these samples to account for this decline. Despite the decline in the light yield, the number of selected neutrino interaction candidates is not significantly impacted. In addition, several systematic uncertainty variation samples have been developed to encompass any potential mis-modelling of the light. The cause of the light yield decline remains a subject of active investigation. Preliminary studies of the contaminants present in the liquid argon (e.g. nitrogen, xenon) performed in collaboration with CIEMAT, as well as further investigations of MicroBooNE's data-set, are contributing to making an informed assessment of the possible causes of the decline. Understanding the long-term performance of scintillation light is critical for operation of upcoming LArTPCs, and MicroBooNE's experience and findings provide valuable insight for future LArTPC operations.

References

[1] E. Morikawa, R. Reininger, P. Gürtler, V. Saile, and P. Laporte. Argon, krypton, and xenon excimer luminescence: From the dilute gas to the condensed phase. *The Journal of Chemical Physics*, 91(3):1469–1477, 1989. doi:10.1063/1.457108.

[2] P. Abratenko et al. Search for an Excess of Electron Neutrino Interactions in MicroBooNE Using Multiple Final-State Topologies. *Phys. Rev. Lett.*, 128(24):241801, 2022. doi:10.1103/PhysRevLett.128.241801.

[3] R. Acciarri et al. Design and Construction of the MicroBooNE Detector. *JINST*, 12 (02):P02017, 2017. doi:10.1088/1748-0221/12/02/P02017.

[4] The MicroBooNE Collaboration. PMT Gain Calibration In MicroBooNE. 8 2019. doi:10.2172/1573228. URL https://microboone.fnal.gov/wp-content/uploads/MICROBOONE-NOTE-1064-TECH.pdf.

[5] P. Abratenko et al. Measurement of space charge effects in the MicroBooNE LArTPC using cosmic muons. *JINST*, 15(12):P12037, 2020. doi:10.1088/1748-0221/15/12/P12037.

[6] The MicroBooNE Collaboration. Measuring Light Yield with Isolated Protons in MicroBooNE. 9 2022. URL https://microboone.fnal.gov/wp-content/uploads/MICROBOONE-NOTE-1119-PUB.pdf.

[7] R. Acciarri et al. Effects of Nitrogen contamination in liquid Argon. *JINST*, 5:P06003, 2010. doi:10.1088/1748-0221/5/06/P06003.

[8] R. Acciarri et al. Oxygen contamination in liquid Argon: Combined effects on ionization electron charge and scintillation light. *JINST*, 5:P05003, 2010. doi:10.1088/1748-0221/5/05/P05003.

[9] B. J. P. Jones, C. S. Chiu, J. M. Conrad, C. M. Ignarra, T. Katori, and M. Toups. A Measurement of the Absorption of Liquid Argon Scintillation Light by Dissolved Nitrogen at the Part-Per-Million Level. *JINST*, 8:P07011, 2013. doi:10.1088/1748-0221/8/07/P07011. [Erratum: JINST 8, E09001 (2013)].

[10] B. J. P. Jones, T. Alexander, H. O. Back, G. Collin, J. M. Conrad, A. Greene, T. Katori, S. Pordes, and M. Toups. The Effects of Dissolved Methane upon Liquid Argon Scintillation Light. *JINST*, 8:P12015, 2013. doi:10.1088/1748-0221/8/12/P12015.

[11] J. Calvo et al. Measurement of the attenuation length of argon scintillation light in the ArDM LAr TPC. *Astropart. Phys.*, 97:186–196, 2018. doi:10.1016/j.astropartphys.2017.11.009.

[12] Roberto Santorelli. Analysis of the argon purity by icpms. 2022. URL https://indico.sanfordlab.org/event/29/contributions/431/attachments/366/882/Santorelli_LRT2022.pdf.

[13] M. Babicz et al. A measurement of the group velocity of scintillation light in liquid argon. *JINST*, 15(09):P09009, 2020. doi:10.1088/1748-0221/15/09/P09009.

[14] P. Abratenko et al. Search for an anomalous excess of charged-current νe interactions without pions in the final state with the MicroBooNE experiment. *Phys. Rev. D*, 105 (11):112004, 2022. doi:10.1103/PhysRevD.105.112004.